

ORIGINAL ARTICLE

The assessment of time dependent flow of Williamson fluid with radiative blood flow against a wedge

K. Subbarayudu^a, S. Suneetha^a, P. Bala Anki Reddy^{b,*}

^aDepartment of Applied Mathematics, Yogi Vemana University, Kadapa, 516005, India

^bDepartment of Mathematics, S.A.S., Vellore Institute of Technology, Vellore, 632014, India

Received 17 July 2018; accepted 16 July 2019

Available online XXXX

KEYWORDS

Williamson fluid model;
Wedge shape geometry;
Magnetohydrodynamic
(MHD);
Thermal radiation;
Blood flow

Abstract The present pagination reports both Brownian diffusion and thermophoresis aspects subject to magneto hydrodynamic Williamson fluid model. Assuming the flow is unsteady and blood is treated as Williamson fluid over a wedge with radiation. The governing equations are transformed into ordinary differential equations by using similarity variables. The analytical solutions of the transformed governing equations are obtained by using the MATLAB bvp4c solver. The effects of various physical parameters such as Hartmann number, local Weissenberg number, radiation parameter, unsteadiness parameter, Prandtl number, Lewis number, Brownian diffusion, thermophoresis, wedge angle parameter, moving wedge parameter, on velocity, temperature, concentration, skin friction, heat transfer rate and mass transfer rate have been discussed in detail. The velocity and temperature profile deprives for larger We and an opposite trend is observed for concentration. The radiation parameter is propositional to temperature and a counter behavior is observed for Pr .

© 2019 Beihang University. Production and hosting by Elsevier B.V. on behalf of KeAi. This is an open access article under the CC BY-NC-ND license (<http://creativecommons.org/licenses/by-nc-nd/4.0/>).

*Corresponding author.

E-mail address: pbarmaths@gmail.com (P. Bala Anki Reddy).

Peer review under responsibility of Beihang University.



1. Introduction

Till date, researchers are doing lots of experimental and theoretical investigations to study the non-Newtonian fluid models because of their significant applications in several biological and industrial processes. The theory of non-

Nomenclature

A	unsteadiness parameter
B	magnetic field (unit: $\text{kg}\cdot\text{s}^{-2}\cdot\text{A}^{-1}$)
B_0	magnetic field strength (unit: A/m)
C	concentration
C_w	concentration at the surface
C_∞	ambient concentration
C_0	initial reference concentration
C_p	specific heat (unit: $\text{J}\cdot\text{kg}^{-1}\cdot\text{K}^{-1}$)
C_{fx}	local skin friction coefficient
D_B	Brownian diffusion coefficient (unit: $\text{m}^2\cdot\text{s}^{-1}$)
D_T	thermophoretic diffusion coefficient (unit: $\text{m}^2\cdot\text{s}^{-1}$)
f	dimensionless stream function
Ha	Hartmann number
k^*	Rosseland mean absorption coefficient (unit: m^{-1})
Le	Lewis number
M	stretching parameter (unit: s^{-1})
Nb	Brownian motion parameter
Nt	thermophoresis parameter
Nu_x	local Nusselt number
Pr	Prandtl number
q_s	wall mass flux (unit: $\text{kg}\cdot\text{m}^{-2}\cdot\text{s}^{-1}$)
q_r	radiative heat flux (unit: $\text{W}\cdot\text{m}^{-2}$)
q_w	wall heat flux (unit: $\text{W}\cdot\text{m}^{-2}$)
Re_x	local Reynolds number
Rd	radiation parameter
Sh_x	local Sherwood number
T	temperature (unit: K)
T_0	initial reference temperature
T_w	temperature at the surface (unit: K)

T_∞	ambient temperature
u	velocity component along x direction (unit: $\text{m}\cdot\text{s}^{-1}$)
u_w	stretching sheet velocity (unit: $\text{m}\cdot\text{s}^{-1}$)
u_e	free stream velocity (unit: $\text{m}\cdot\text{s}^{-1}$)
v	velocity component along y direction (unit: $\text{m}\cdot\text{s}^{-1}$)
We	local Weissenberg number

Greek symbols

A	wedge moving parameter
σ	electrical conductivity (unit: $\text{S}\cdot\text{m}^{-1}$)
ρ	fluid density (unit: $\text{kg}\cdot\text{m}^{-3}$)
γ	shear rate
ϕ	dimensionless concentration
θ	dimensionless temperature
ν	kinematic coefficient of viscosity (unit: $\text{m}^2\cdot\text{s}^{-1}$)
ψ	stream function (unit: $\text{m}^2\cdot\text{s}$)
η	similarity variable
M	generalized Newtonian viscosity
μ_0	zero shear viscosity (unit: $\text{N}\cdot\text{s}\cdot\text{m}^{-2}$)
μ_∞	infinity shear viscosity (unit: $\text{N}\cdot\text{s}\cdot\text{m}^{-2}$)
σ^*	Stefan Boltzmann constant (unit: $\text{W}\cdot\text{m}^{-2}\cdot\text{K}^{-4}$)
τ_w	wall shear stress (unit: $\text{N}\cdot\text{m}^{-2}$)
Γ	material constants
A	effective thermal diffusivity (unit: $\text{m}\cdot\text{s}^{-1}$)
A	wedge moving parameter
B	wedge angle parameter
β^*	ratio of viscosities
Ω	total wedge angle
κ	thermal conductivity (unit: $\text{W}\cdot\text{m}^{-1}\cdot\text{K}^{-1}$)

Newtonian fluids are much considered when compared to Newtonian fluids due to vast engineering applications, for instance, emulsions, lubricants, bio-fluids in biological tissue and polymers, biomedical fluids and nuclear fuel slurries. Depending upon the various rheological features of non-Newtonian fluids, so many rheological models have been modeled. Some existing models are: power law model, Carreau model, Jeffery fluid model, cross model, Ellis model, Sisko model and Williamson fluid model etc. Out of these, Williamson fluid model is simple model to simulate the viscoelastic shear thinning characteristics of non-Newtonian fluids.

Williamson fluid model report the flow of shear thinning non-Newtonian fluids. This model was introduced by Williamson [1] in 1929 and he gave the experimental results. In Williamson fluid model, the effective viscosity should lessen indefinitely with rising shear rate, which is nothing but an infinite viscosity at stationary (zero fluid motion) and nil viscosity as the shear rate tend to infinity. Nadeem et al. [2] proposed the momentum, heat and mass transfer effect of non-Newtonian Williamson fluid towards stretching sheet with various physical parameters. Few current explorations on Williamson fluid are disclosed in Refs. [3,4]. Khan et al. [5] studied Williamson fluid flow with chemically reactive species using scaling conversion and homotopy analysis method. Nadeem and Hussain [2] analyzed Williamson fluid

flow and thermal energy analysis over exponentially stretching surface, (PEST) and (PEHF) case. The mathematical expression of Williamson constitutive model is expressed as $\mu = \mu_\infty + (\mu_0 - \mu_\infty)[1 - \Gamma\gamma]^{-1}$, in which (μ_0) and (μ_∞) are the zero and infinite shear rate viscosities, respectively, Γ is a material constant. The shear rate is defined as $\gamma = \sqrt{\frac{1}{2} \sum_i \sum_j \gamma_{ij} \gamma_{ji}}$. Due to the prominence ap-

plications in biological phenomenon, the peristaltic flow and heat transfer analysis of Williamson fluid have fascinated.

Over the last many years, the flow and heat transfer analysis past wedge-shaped bodies has been a matter of utmost synchronic interest in the field of engineering and chemical industry. For example, in the fields of aerodynamics, hydrodynamics, heat exchangers, ground water pollution, thermal insulation, geothermal systems, etc. Particularly such flows occur often in enhanced oil recovery, aircraft response to atmospheric gusts, packed bed reactor geothermal industries, ground water pollution and so forth. A wedge is a triangular shaped tool, and is a portable inclined plane, and one of the six classical simple machines. It can be used to separate two objects or portions of an object, lift up an object, or hold an object in place. It converts the lateral force into a transverse splitting force. Numerical investigation was done by Amir Hamid et al. [6] on heat

transfer performance in time dependent flow of Williamson fluid past a wedge-shaped geometry. Hashim et al. [7] investigated an unsteady heat and mass transfer flow of Williamson nanofluid along a wedge and further depicts that the rate of heat transfer is accelerated with the growth in Brownian motion and thermophoresis parameter Tanveer et al. [8] focused on the assessment of nanofluid in a Von Karman flow with temperature relied viscosity and shows that the temperature and concentration distributions give opposite response towards large Brownian motion parameter, and reduction in local Nusselt number is noticed with an increase in Brownian motion Nb and thermophoresis Nt .

In nature magnetic field exists everywhere, it follows that magnetohydrodynamic (MHD) phenomena must occur whenever conducting fluids are available. It has many engineering applications, in the fields of aeronautics, planetary and stellar magnetospheres, solar physics, cosmic fluid dynamics, electronics, chemical engineering, MHD generators, MHD accelerators, construction of turbines, and other centrifugal machines. When a magnetic field is applied to a moving and electrically conducting fluid, electric and magnetic fields are induced. These fields interact with each other, a body force known as Lorentz force is produced, which slows down the motion of fluid. Bala Anki Reddy et al. [9] analyzed the magnetohydrodynamics boundary layer slip flow of a Maxwell nano fluid over an exponentially stretching surface with convective boundary condition. Khan and Hashim [10] studied the effects of multiple slip on flow of magneto-Carreau fluid along wedge with chemically reactive species and investigated that there is a raise in the shear stress and the fluid velocity by raising the magnetic parameter, while the temperature and concentration profiles are decelerated. More recently various sleuths [11–14] studied on MHD with different fluid flows. Imran Ullah et al. [15] upshot on the heat and mass transfer in unsteady MHD slip flow of Casson fluid over a moving wedge and also noticed that unsteadiness parameter thinning the velocity boundary layer while opposite to this was found in the thermal and concentration boundary layers.

Thermal radiation plays a vital role in physics and engineering mainly in space technology and high temperature process. Some of these applications include nuclear power plants, gas turbines, polymer processing industry and the various propulsion devices for missiles, aircraft, space vehicles and satellites. Hashim et al. [16] focused on the thermal radiation effects on Williamson fluid flow due to an expanding/contracting cylinder with nanomaterials. Khan and Hamid [17] analyzed on the influence of non-linear thermal radiation on 2D time dependent flow of a Williamson fluid with heat source/sink. Khan et al. [18] managed to establish the MHD boundary layer radiative, heat generating and chemical reacting flow past a wedge moving in a nanofluid. Hydromagnetic boundary layer flow of Williamson fluid in the presence of thermal radiation and Ohmic dissipation was examined by Hayat et al. [19].

Fluid mechanics is a science of materials which are in motion. If blood is considered as a fluid, then the equation

of motion can be modified and can be used to know the mechanical properties and the flow characteristics of blood, which help bioengineers who are busy in designing artificial organs and finding solutions to diseases and disorders of human body which are related human physiology. Blood is a suspension of numerous cells - red blood cells (erythrocytes), white blood cells (leukocytes), and platelets in a liquid electrolyte solution called plasma.

Many researchers have reported that the blood is an electrically conducting fluid. The electromagnetic force (Lorentz force) acts on the blood and this force opposes the motion of blood and there by flow of blood is impeded, so that the external magnetic field can be used in the treatment of some kinds of diseases like cardiovascular diseases and in the diseases with accelerated blood circulation such as haemorrhages and hypertension. Application of magnetic field plays significant role due to its realistic applications in MRI, cancer therapy. Human body experiences magnetic fields of moderate to high intensity in many situations of day to day life.

Blood flow with radiation effect has significant applications in Biomedical engineering and in numerous medical treatment methods namely, thermal therapeutic procedures. Infrared radiation is a technique chosen in heat therapy, as it is possible to directly heat the blood capillaries of the affected areas of the body. Heat therapy is used in the treatment of muscle spasms, myalgia (muscle pain), chronic widespread pain and long-lasting shortening of muscle. Some contribution on this topic with exciting models have been prepared by Srinivas et al. [20], Reddy et al. [21] and Noreen Sher Akbar et al. [22] published in current years.

An understanding of convection heat transfer of fluids is crucial to the design of several types of thermal equipment. From this viewpoint, heat transfer problems of this type have been investigated by a large number of researchers. It is noted through the survey of literature that little information is available on the unsteady flow of Williamson fluid model for a blood flow over a wedge with radiation. Motivated by these applications, the present study explores the influence of Brownian motion and thermophoresis effect of Williamson fluid model for a radiating blood flow over a wedge. To the best of our knowledge no investigation has been made to study the blood flow by treating blood as Williamson fluid.

2. Description of physical model

We presume a two-dimensional, viscous, unsteady, MHD, flow of non-Newtonian Williamson fluid model due to a stretching wedge. The stretching velocity of the wedge is denoted by $u_w(x, t) = \frac{bx^m}{1-ct}$, in which b is the stretching rate and c denote a constant having dimension $(\text{time})^{-1}$. In addition the flow moves along the axis of wedge in the upward direction with a free stream velocity $u_e(x, t) = \frac{ax^m}{1-ct}$, where a , c and m are positive constants with $0 \leq m \leq 1$. The wedge angle is assumed to be $\Omega = \beta\pi$, where $\beta = \frac{2m}{m+1}$

is related to the pressure gradient. The fluid is assumed to be gray, absorbing, emitting but non-scattering. A uniform magnetic field is applied in the direction perpendicular to the wedge. The transverse applied magnetic field and magnetic Reynolds number are assumed to be very small, the induced magnetic field, the external electric field, and the electric field due to the polarization of charges are negligible. An external time dependent magnetic field $B(t) = \frac{B_0}{\sqrt{(1-ct)}}$ is applied normal to the wedge surface. The Cartesian coordinate system is taken for this analysis in such a way x - axis is coinciding with the stretching geometry and y - axis is normally outward to it. A geometrical configuration and schematic model of the present physical model is displayed in Figure 1. To investigate the heat transfer, we have taken the temperature and concentration at the surface of wedge as $T_w(x, t) = T_\infty + \frac{T_0 u_w(x, t)}{v\sqrt{1-ct}}$, $C_w(x, t) = C_\infty + \frac{C_0 u_w(x, t)}{v\sqrt{1-ct}}$, T_0, C_0 represent the initial reference temperature and concentration and also, when y approaches infinity, the free stream attains the constants values T_∞, C_∞ . Then, in the absence of input electric field, under the boundary layer assumption, the continuity equations are given as:

$$\frac{\partial u}{\partial x} + \frac{\partial v}{\partial y} = 0 \quad (1)$$

The momentum equation after employing usual boundary layer for Williamson fluid without viscous dissipation and external force is written as [3,17,23]:

$$\begin{aligned} \frac{\partial u}{\partial t} + u \frac{\partial u}{\partial x} + v \frac{\partial u}{\partial y} = \frac{\partial u_e}{\partial t} + v \frac{\partial^2 u}{\partial y^2} & \left[\beta^* + (1-\beta^*) \left(1 - \Gamma \frac{\partial u}{\partial y} \right)^{-1} \right] \\ + v \Gamma \left(\frac{\partial u}{\partial y} \right) \frac{\partial^2 u}{\partial y^2} & \left[(1-\beta^*) \left(1 - \Gamma \frac{\partial u}{\partial y} \right)^{-2} \right] - \frac{\sigma B^2(t)}{\rho} (u - u_e) \end{aligned} \quad (2)$$

The energy equation for time dependent flow is expressed by:

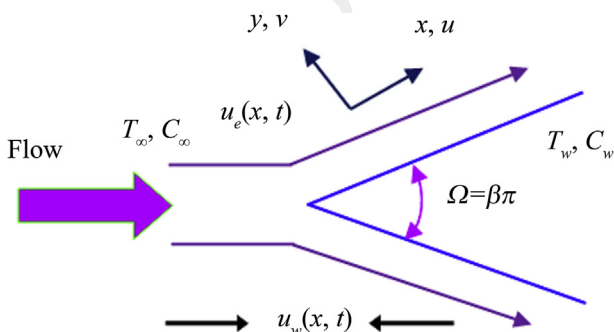


Figure 1 Flow geometry.

$$\begin{aligned} \frac{\partial T}{\partial t} + u \frac{\partial T}{\partial x} + v \frac{\partial T}{\partial y} = \alpha \frac{\partial^2 T}{\partial y^2} - \frac{1}{(\rho c)_f} \frac{\partial q_r}{\partial y} \\ + \tau \left[D_B \frac{\partial C}{\partial y} \frac{\partial T}{\partial y} + \frac{D_T}{T_\infty} \left(\frac{\partial T}{\partial t} \right)^2 \right] \end{aligned} \quad (3)$$

The concentration equation for time dependent flow is expressed by:

$$\frac{\partial C}{\partial t} + u \frac{\partial C}{\partial x} + v \frac{\partial C}{\partial y} = D_B \frac{\partial^2 C}{\partial y^2} + \frac{D_T}{T_\infty} \frac{\partial^2 T}{\partial y^2} \quad (4)$$

It is important to note here that the governing partial differential Eq. (2) of Williamson fluid flow reduces to viscous fluid case when

$$\beta^* = 0 = \Gamma$$

Applying Rosseland approximation for optically thick fluid, the radiative heat flux q_r is given as

$$q_r = -\frac{4\sigma^*}{3k^*} \frac{\partial T^4}{\partial y} \quad (5)$$

One can linearize the nonlinear term T^4 occurring in Eq. (5) with the help of Taylor series by assuming a small variation between the fluid temperature within the boundary layer and ambient fluid temperature, retaining terms up to first order only. Thus T^4 is represented as:

$$T^4 \cong 4T_\infty^3 T - 3T_\infty^4 \quad (6)$$

The modified energy Eq. (3), after incorporating Eqs. (5) and (6), is given by

$$\begin{aligned} \frac{\partial T}{\partial t} + u \frac{\partial T}{\partial x} + v \frac{\partial T}{\partial y} = \alpha \frac{\partial^2 T}{\partial y^2} + \frac{16\sigma^* T_\infty^3}{3\rho c_p k^*} \frac{\partial^2 T}{\partial y^2} \\ + \tau \left[D_B \frac{\partial C}{\partial y} \frac{\partial T}{\partial y} + \frac{D_T}{T_\infty} \left(\frac{\partial T}{\partial t} \right)^2 \right] \end{aligned} \quad (7)$$

2.1. Boundary conditions

We have applied the no-slip condition at the surface of the wedge and other flow conditions for the physical model are given as follows:

(a) On the wedge surface i.e., at $y=0$:

$$u = u_w = u_e(x, t), \quad v = 0, \quad T = T_w(x, t), \quad C = C_w(x, t), \quad (8)$$

(b) At free stream i.e., as $y \rightarrow \infty$

$$u \rightarrow u_e, \quad T \rightarrow T_\infty, \quad C \rightarrow C_\infty \quad (9)$$

2.2. Method of solution

To construct the flow model dimensionless, let us use the following non-dimensional quantities [24]:

$$\eta = y\sqrt{\frac{(m+1)u_e}{ux}}, \quad \psi = \sqrt{\frac{2uxu_e}{m+1}}f(\eta),$$

$$\theta(\eta) = \frac{T - T_\infty}{T_w - T_\infty}, \quad \phi(\eta) = \frac{C - C_\infty}{C_w - C_\infty},$$
(10)

Here, the Stokes stream function $\psi(x, y, t)$ identically satisfies the continuity Eq. (1). The velocity components are then given by $u = \frac{\partial\psi}{\partial y}$ and $v = -\frac{\partial\psi}{\partial x}$ respectively. By substituting the above mentioned non-dimensional parameters into Eqs. (2), (4) and (7) we get the corresponding nonlinear ordinary differential conditions:

$$[\beta^* + (1 - \beta^*)(1 - We f''')^{-2}]f'''' + f f'''' + \beta(1 - (f')^2) - A(2 - \beta)(f' + \frac{\eta}{2}f'' - 1) - Ha^2(2 - \beta)\{f' - 1\} = 0,$$
(11)

$$\frac{1}{Pr} \left[1 + \frac{4}{3}Rd \right] \theta'' + (f\theta' - 2f'\theta) - \frac{A}{2}(2 - \beta)(\eta\theta' + 3\theta) + Nb\theta'\phi' + Nt\theta^2 = 0,$$
(12)

$$\frac{1}{Le} \left[\phi'' + \frac{Nt}{Nb}\theta'' \right] - \frac{A}{2}(2 - \beta)(\eta\phi' + 3\phi) - 2f'\phi + f\phi' = 0,$$
(13)

with reduced boundary conditions:

$$f(0) = 0, \quad f'(0) = \lambda, \quad \theta(0) = 1, \quad \phi(0) = 1$$
(14)

$$f'(\infty) \rightarrow 1, \quad \theta(\infty) \rightarrow 0, \quad \phi(\infty) \rightarrow 0$$
(15)

Here, $\lambda = \frac{b}{a}$ denote the wedge moving parameter and $\lambda > 0$ means a stretching wedge and $\lambda < 0$ specify a shrinking wedge while $\lambda = 0$ for a static wedge.

The other involve physical dimensionless quantities are given by:

$\beta^* = \frac{\mu_0}{\mu_\infty}$ is the ratio of viscosities, $\alpha = \frac{\kappa}{\rho C_p}$ is the effective thermal diffusivity, $We = \sqrt{\frac{\Gamma^2(m+1)\mu_e^3}{2ux}}$ is the local Weissenberg number, $Pr = \frac{\rho C_p}{k}$ is the Prandtl number, $Rd = \frac{4\sigma^* T_\infty^3}{kk_1}$ is the radiation parameter, $A = \frac{c}{\alpha x^{m-1}}$ is the unsteadiness parameter and $\beta = \frac{2m}{m+1}$ is the wedge angle parameter, $Ha^2 = \frac{\rho B_0^2}{\rho \alpha x^{m-1}}$ is the Hartmann number, $Le = \frac{v}{D_B}$ is the Lewis number, $Nt = \frac{\tau D_T (T_w - T_\infty)}{T_\infty v}$ is the thermophoresis parameter, $Nb = \frac{\tau D_B (C_w - C_\infty)}{v}$ is the Brownian motion parameter.

Table 1 A comparison of numerical results of $-f''(0)$ for different β when $\beta^* = We = \lambda = Ha = A = 0$.

β	Ishaq [25]	Rajgopal [26]	Kuo [27]	Aamir Hamid et al. [6]	Present study
0.0	0.4696	—	0.469600	0.469600	0.4696
0.1	0.5870	0.5870	0.587080	0.587035	0.5869
0.3	0.7748	0.7747	0.774724	0.774755	0.7747
0.5	0.9277	0.9276	0.927905	0.927680	0.8543
0.9	1.2326	1.2325	1.232589	1.232588	0.9392

2.3. Engineering parameters

The imperative physical parameters of engineering concern in materials processing operations are the local non-dimensional friction factor C_{fx} , Nusselt number Nu_x and Sherwood number Sh_x . By their definitions, we have

$$C_{fx} = \frac{\tau_w}{\rho U_w^2}, \quad Nu_x = \frac{xq_w}{k(T_w - T_\infty)} \quad \text{and} \quad Sh_x = \frac{xq_m}{D_B(C_w - C_\infty)}$$

where τ_w , q_w and q_m are given as

$$\tau_w = \mu_0 \left(\frac{\partial u}{\partial y} \right) \left[\beta^* + (1 - \beta^*) \left(1 - \Gamma \frac{\partial u}{\partial y} \right)^{-1} \right]_{y=0},$$

$$q_w = - \left[\left(k + \frac{16\sigma T^3}{3k^*} \right) \frac{\partial T}{\partial y} \right]_{y=0} \quad \text{and} \quad q_m = - D_B \left(\frac{\partial C}{\partial y} \right)_{y=0}$$
(16)

In view of Eqs. (10) and (16), the dimensionless local skin friction, local Nusselt number and local Sherwood number are given by

Table 2 The numerical data of skin friction coefficient, local Nusselt number and local Sherwood number for various values of $\beta, \lambda, We, \beta^*, Ha, A$ when $Pr = 21, Nb = 0.5, Nt = 0.5, Rd = 0.5, Le = 0.5$.

β	λ	We	β^*	Ha	A	$f''(0)$	$-\theta'(0)$	$-\phi'(0)$
0.2	0.1	0.5	0.2	0.5	1.0	0.5474	1.7642	0.7564
0.3	0.1	0.5	0.2	0.5	1.0	0.5528	1.7003	0.7536
0.4	0.1	0.5	0.2	0.5	1.0	0.5581	1.6337	0.7508
0.5	0.1	0.5	0.2	0.5	1.0	0.5681	1.5645	0.7477
0.2	0.2	0.5	0.2	0.5	1.0	0.5635	1.6524	0.8421
0.2	0.3	0.5	0.2	0.5	1.0	0.4814	1.5385	0.9265
0.2	0.4	0.5	0.2	0.5	1.0	0.4081	1.4229	1.0097
0.2	0.1	0.6	0.2	0.5	1.0	0.4266	1.7690	0.7501
0.2	0.1	0.7	0.2	0.5	1.0	0.4057	1.7731	0.7441
0.2	0.1	0.8	0.2	0.5	1.0	0.2699	1.7770	0.7383
0.2	0.1	0.5	0.3	0.5	1.0	0.1396	1.7632	0.7587
0.2	0.1	0.5	0.4	0.5	1.0	0.6187	1.7614	0.7612
0.2	0.1	0.5	0.5	0.5	1.0	0.6929	1.7595	0.7640
0.2	0.1	0.5	0.2	1.0	1.0	0.7709	1.8730	0.7656
0.2	0.1	0.5	0.2	1.5	1.0	0.5655	1.9756	0.7750
0.2	0.1	0.5	0.2	2.0	1.0	0.5827	2.0735	0.7846
0.2	0.1	0.5	0.2	0.5	1.1	0.5992	1.7523	0.7758
0.2	0.1	0.5	0.2	0.5	1.2	0.6961	1.7399	0.7945
0.2	0.1	0.5	0.2	0.5	1.3	0.8521	1.7295	0.8097

$$C_{fx} Re_x^{1/2} = \frac{1}{\sqrt{2-\beta}} f''(0) [\beta^* + (1-\beta^*)\{1 - We f''(0)\}^{-1}],$$

$$Nu_x Re_x^{-1/2} = -\frac{1}{\sqrt{2-\beta}} \theta'(0) \quad \text{and}$$

$$Sh_x Re_x^{-1/2} = -\frac{1}{\sqrt{2-\beta}} \phi'(0),$$

(17)

where $Re_x = \frac{U_\infty x}{\nu}$ represents the local Reynolds number.

2.4. Numerical approach and validation

The non-dimensional system of Eqs. (11)–(13) along with boundary conditions (14)–(15) have been tackled numerically by applying shooting procedure with RKF 4–5th order of integration formula. For this scheme, we first modify the primary differential equations into a set of first order ODEs.

$$\begin{aligned} f &= y_1, & f' &= y_2, & f'' &= y_3, & f''' &= y'_3, \\ \theta &= y_4, & \theta' &= y_5, & \theta'' &= y'_5, & \phi &= y_6, & \phi' &= y_7, & \phi'' &= y'_7. \end{aligned}$$

Now we get first order system of equations:

$$\begin{bmatrix} y'_1 \\ y'_2 \\ y'_3 \\ y'_4 \\ y'_5 \\ y'_6 \\ y'_7 \end{bmatrix} = \begin{bmatrix} y_2 \\ y_3 \\ -\left(\frac{(y_1 y_3 + \beta(1 - y_2^2)) - A(2 - \beta)(y_2 + \frac{\eta}{2} y_3 - 1) - Ha^2(2 - \beta)(y_2 - 1)}{\beta^* + (1 - \beta^*)(1 - We y_3)^{-2}}\right) \\ y_5 \\ -\left(\frac{Pr}{1 + \frac{4}{3} Rd}\right) \left((y_1 y_5 - 2y_2 y_4) - \frac{A}{2}(2 - \beta)(\eta y_5 + 3y_4) + Nb y_5 y_7 + Nt y_5^2\right) \\ y_7 \\ \left(Le \left(\frac{A}{2}(2 - \beta)(\eta - y_5 + 3y_4) + 2y_2 y_6 - y_1 y_7\right)\right) \\ -\frac{1}{Le} \frac{Nt}{Nb} \left(-Pr \left((y_1 y_5 - 2y_2 y_4) - \frac{A}{2}(2 - \beta)(\eta y_5 + 3y_4) + Nb y_5 y_7 + Nt y_5^2\right)\right) \end{bmatrix} \quad (18)$$

Table 3 The numerical data of skin friction coefficient, local Nusselt number and local Sherwood number for various values of Pr, Nb, Nt, Rd, Le , when $\beta = 0.2, \lambda = 0.1, We = 0.5, \beta^* = 0.5, Ha = 0.5, A = 1.0$.

Pr	Nb	Nt	Rd	Le	$f''(0)$	$-\theta'(0)$	$-\phi'(0)$
21	0.5	0.5	0.5	0.5	0.5474	1.7642	0.7564
22	0.5	0.5	0.5	0.5	0.5474	1.7710	0.7540
23	0.5	0.5	0.5	0.5	0.5474	1.7767	0.7519
21	1.0	0.5	0.5	0.5	0.5474	1.3310	1.0954
21	1.5	0.5	0.5	0.5	0.5474	1.0455	1.1871
21	0.5	1.0	0.5	0.5	0.5474	1.3958	0.5398
21	0.5	1.5	0.5	0.5	0.5474	1.3216	0.5060
21	0.5	0.5	1.0	0.5	0.5474	1.7118	0.7761
f21	0.5	0.5	1.5	0.5	0.5474	1.6624	0.7946
21	0.5	0.5	0.5	1.0	0.5474	1.7048	0.9126
21	0.5	0.5	0.5	1.5	0.5474	1.6632	1.0277

The associated initial conditions are:

$$\begin{bmatrix} y_1 \\ y_2 \\ y_3 \\ y_4 \\ y_5 \\ y_6 \\ y_7 \end{bmatrix} = \begin{bmatrix} 0 \\ \lambda \\ q_1 \\ 1 \\ q_2 \\ 1 \\ q_3 \end{bmatrix} \quad (19)$$

The system of first order ODEs (18) with initial conditions (19) is solved using order of fourth-fifth RKF-integration process and suitable values of unknown initial conditions q_1, q_2 and q_3 is preferred and then numerical integration is applied. Here we contrast the computed values of f', θ and ϕ as $\eta \rightarrow \infty$, through the specified boundary

condition $f'(\infty)=1$, $\theta(\infty)=0$ and $\phi(\infty)=0$ and regulate the estimated values of q_1 , q_2 and q_3 to gain an excellent approximation for result. The unknown q_1 , q_2 and q_3 have been approximated by Newton's scheme such a way that boundary conditions suited at highest numerical values of $\eta \rightarrow \infty$, with error less than 10^{-8} .

To prove the validity of the achieved numerical results, a comparison with the existing literature is also conducted in limiting cases. The obtained results of the skin friction coefficient for selected values of the wedge angle parameter are also compared with those described by Ishaq et al. [25], Rajgopal et al. [26], Kuo [27], Amir Hamid et al. [6] (Table 1). An outstanding agreement with the results of the aforesaid authors is noticed.

3. Results and discussions

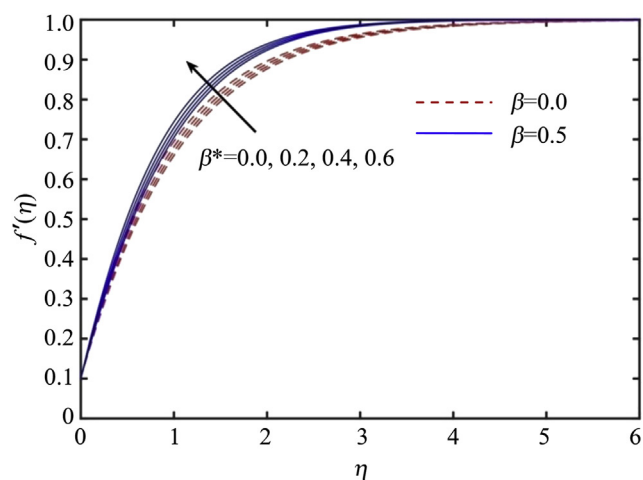
The set of nonlinear ordinary differential Eqs. (11)–(13) with boundary conditions (14) and (15) have been solved using the MATLAB bvp4c solver. Following the work of

Turkylmazoglu [28], numerical simulation is completed by reporting a certain range of required parameters

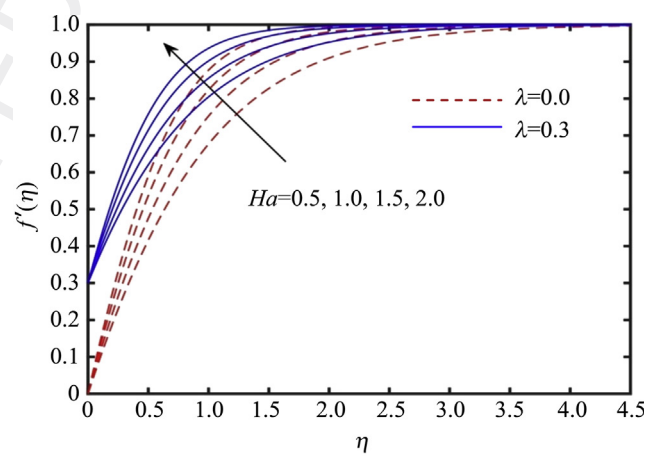
$A(0.0 \leq A \leq 1.2)$, $Ha(0 \leq Ha \leq 3.0)$, $We(1.0 \leq We \leq 4.0)$, $\beta^*(0 \leq \beta^* \leq 1.0)$, $Nt(0.1 \leq Nt \leq 2.5)$, $Nb(0.1 \leq Nb \leq 0.4)$

and $Le(1.0 \leq Le \leq 4.0)$. This section is devoted to analyze effects of the assorted parameters $A = 1.0$, $We = 0.5$, $\beta = 0.2$, $Rd = 0.5$, $Nt = 0.5$, $Nb = 0.5$, $Le = 0.5$, $\lambda = 0.3$, $Ha = 0.5$, involved in the flow problem on flow fields. In the whole analysis these values are kept constant except the varied parameters as shown in the figure legends. Misra and Sinha [29], Valvano et al. [30] and Chato [31] reported the following data for human blood at a temperature $T = 310$ K, $\mu = 3.2 \times 10^{-3}$ kg/(m·s), $C_p = 14.65$ J/(kg·K), $k = 2.2 \times 10^{-3}$ J/(m·s·K), from this, we find that the value of the Prandtl number $Pr = \frac{\rho C_p}{k}$ for human blood is 21 (approximately). The numerical results are depicted in the form of graphs and tables.

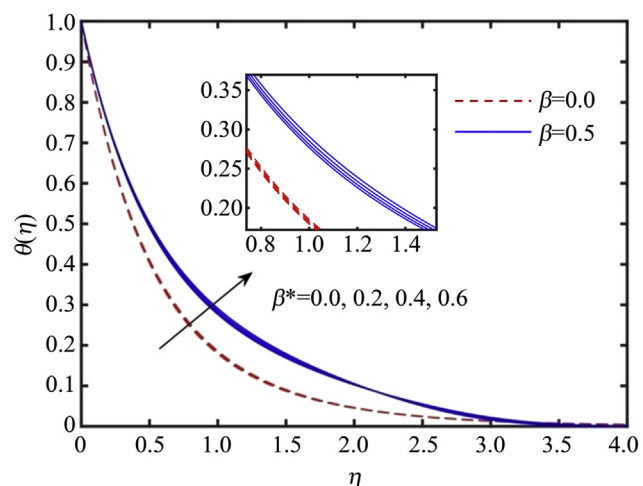
Table 2 points out the behavior of involved physical parameters on skin friction coefficient, local Nusselt number and local Sherwood number. It is seen that skin friction



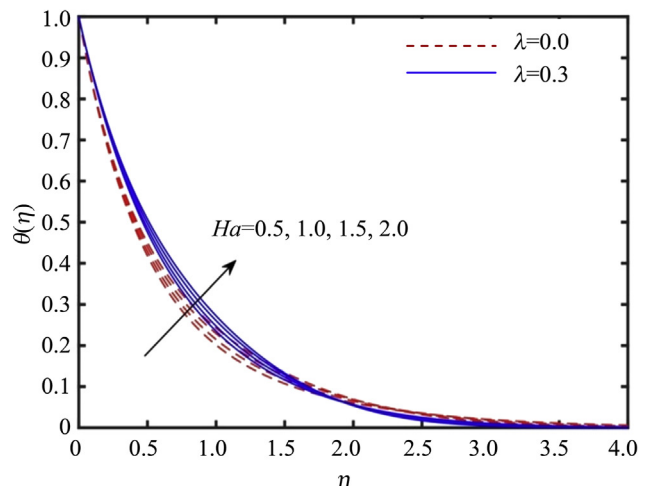
(a) $f'(\eta)$ against β^*



(a) $f'(\eta)$ against Ha



(b) $\theta(\eta)$ against β^*



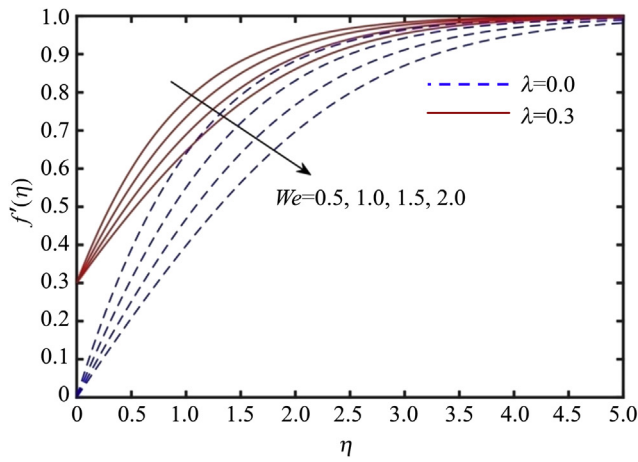
(b) $\theta(\eta)$ against Ha

Figure 2 (a) $f'(\eta)$ against β^* and (b) $\theta(\eta)$ against β^* .

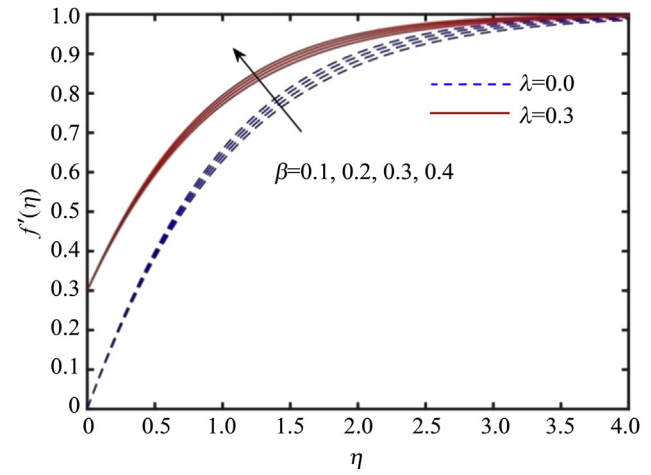
Figure 3 (a) $f'(\eta)$ against Ha and (b) $\theta(\eta)$ against Ha .

coefficient escalates for wedge angle parameter β , viscosity ratio parameter β^* , unsteadiness parameter A , and declines for wedge moving parameter λ , local Weissenberg number

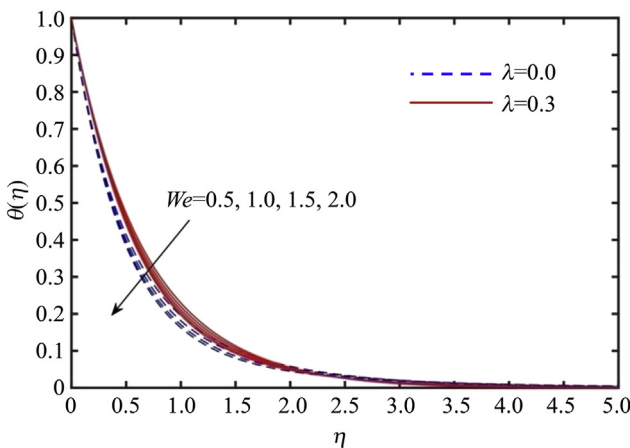
We and Ha . It is inspected that local Nusselt number boost up for local Weissenberg number We , and Ha and a shrinkage is observed for wedge angle parameter β , wedge



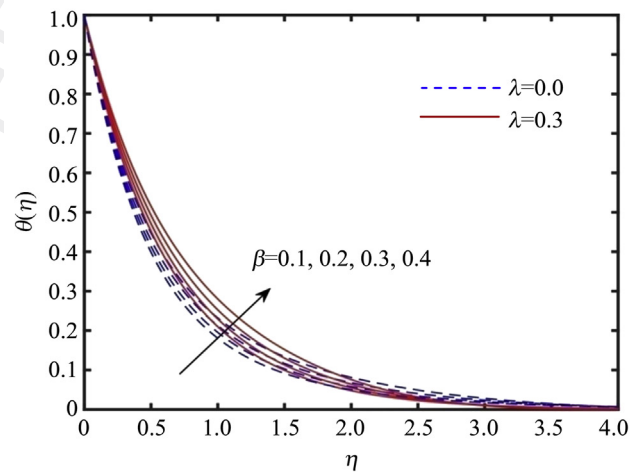
(a) $f'(\eta)$ against We



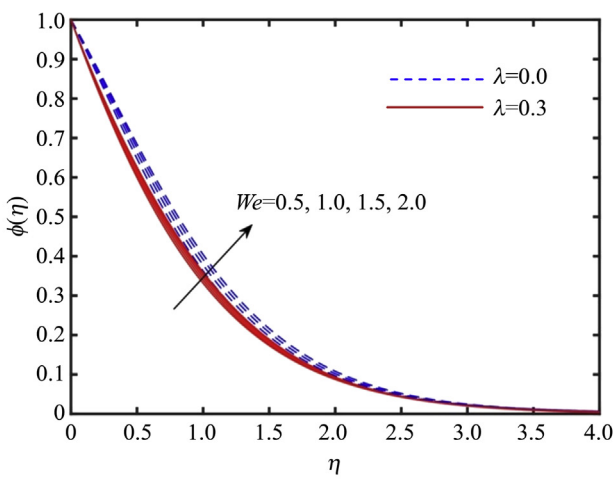
(a) $f'(\eta)$ against β



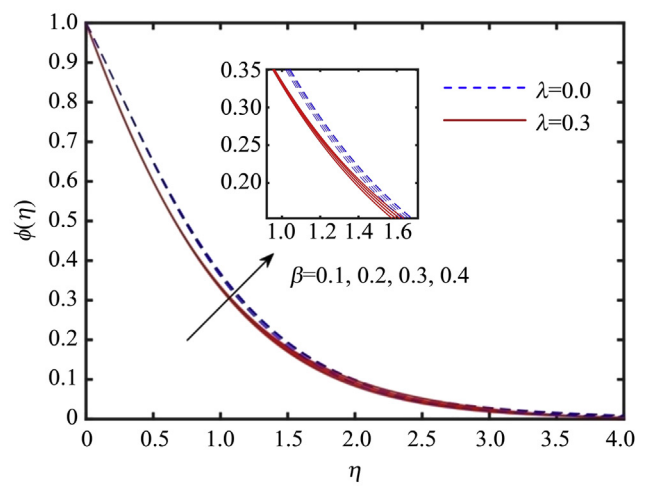
(b) $\theta(\eta)$ against We



(b) $\theta(\eta)$ against β



(c) $\phi(\eta)$ against We



(c) $\phi(\eta)$ against β

Figure 4 (a) $f'(\eta)$ against We , (b) $\theta(\eta)$ against We , and (c) $\phi(\eta)$ against We .

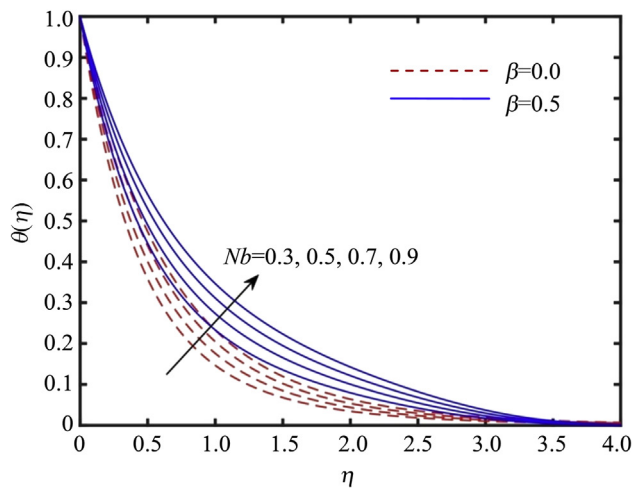
Figure 5 (a) $f'(\eta)$ against β , (b) $\theta(\eta)$ against β , and (c) $\phi(\eta)$ against β .

moving parameter λ , viscosity ratio parameter β^* , unsteadiness parameter A . It is inspected that Sherwood number increases for wedge moving parameter λ , viscosity ratio parameter β^* , unsteadiness parameter A , and a reverse effect is noticed for wedge angle parameter β and local Weissenberg number We .

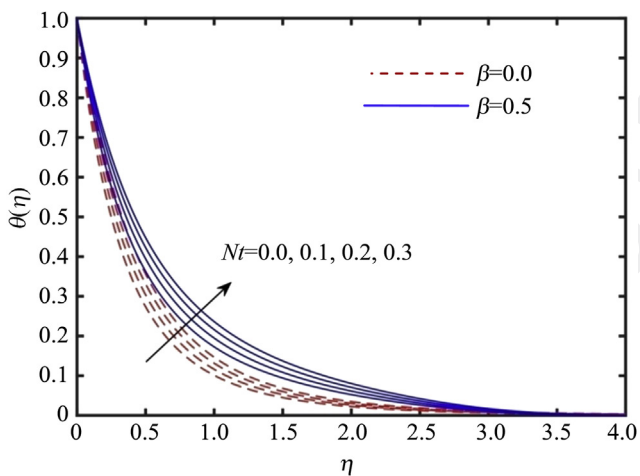
Table 3 points out the behavior of involved physical parameters on skin friction coefficient, local Nusselt number and local Sherwood number. The skin friction coefficient has no impact with increasing values of Pr , Nt , Nb , Rd , Le . The result implies that the Nusselt number increases with the increase in Prandtl number Pr but the increment of thermophoresis parameter Nt , Brownian motion parameter Nb , Radiation parameter Rd , and Lewis number Le reduces the local Nusselt number. An increase in the Sherwood number by the increase in Brownian motion parameter Nb , thermophoresis parameter Nt , Lewis number Le and Brownian motion parameter Nb . But the enhancement of the Prandtl number Pr and thermophoresis parameter Nt reduces the local Sherwood number.

3.1. The effect of viscosity ratio parameter

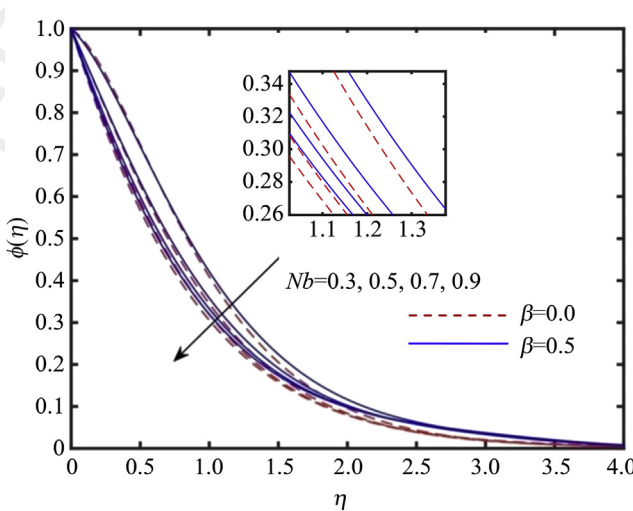
Figure 2(a), (b) are displayed to get insight of the physical behavior of viscosity ratio parameter β^* on



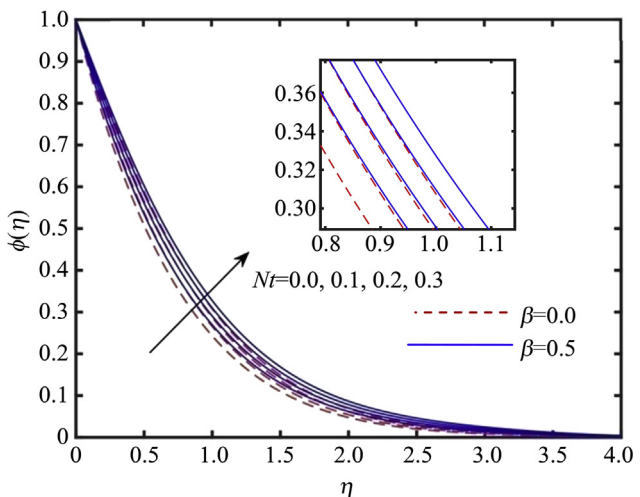
(a) $\theta(\eta)$ against Nb



(a) $\theta(\eta)$ against Nt



(b) $\phi(\eta)$ against Nb



(b) $\phi(\eta)$ against Nt

Figure 7 (a) $\theta(\eta)$ against Nb and (b) $\phi(\eta)$ against Nb .

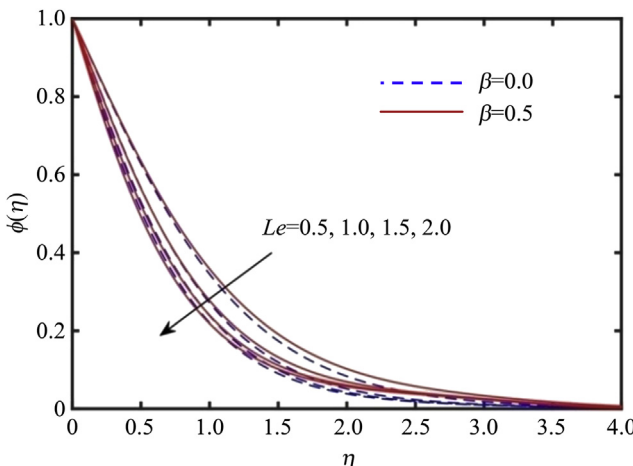


Figure 8 $\phi(\eta)$ against Le .

Figure 6 (a) $\theta(\eta)$ against Nt and (b) $\phi(\eta)$ against Nt .

63
64
65
66
67
68
69
70
71
72
73
74
75
76
77
78
79
80
81
82
83
84
85
86
87
88
89
90
91
92
93
94
95
96
97
98
99
100
101
102
103
104
105
106
107
108
109
110
111
112
113
114
115
116
117
118
119
120
121
122
123
124

velocity and temperature profiles. Both the Figures exhibit that fluid velocity and the momentum boundary layer thickness is higher for increasing values of β^* . It is important to note that $\beta > 0$ show the favorable pressure gradient and $\beta < 0$ reveal an opposing pressure gradient. Further, $m=0$ ($\beta=0$) implies the fluid flow past a flat plate (wedge angle of zero degree) and $m=1$ ($\beta=1$) means the stagnation point flow (wedge angle of 90°). It is also observed that the fluid velocity is higher for the flow near stagnation point when compared with flow over a flat plate.

3.2. The effect of Hartmann number

The effect of Hartmann number on momentum and thermal boundary layers are disseminated in Figure 3(a)(b). Physically, $Ha > 0$ stands for hydromagnetic flow and $Ha=0$ depicts hydrodynamic flow. From Figure 3(a) we clearly see that the velocity profiles in the flow field enhances with the increase of Ha . Moreover, the imposed magnetic field creates Lorenz force which tends to deliver resistance in momentum of liquid particles because of which momentum boundary layer moves towards surface. It is analyzed that the velocity boundary layer thickness decreases for higher Ha for both the cases i.e., flow over a static and moving wedge. In view of physics, the Lorenz force generated by the twin actions electric and magnetic fields lessens the momentum boundary layer thickness by resisting the transport phenomenon. Figure 3(b) displays the impact of Ha on temperature profile. An increasing trend is observed in this profile for both cases $\lambda=0$ or $\lambda=0.3$.

3.3. The effect of Weissenberg number

The behavior of local Weissenberg number on non-dimensional velocity, temperature and concentration are delineated in Figure 4(a)–(c). The profiles of $f'(\eta)$ and momentum boundary layer depreciates for higher estimation of Weissenberg number in case of both static and moving

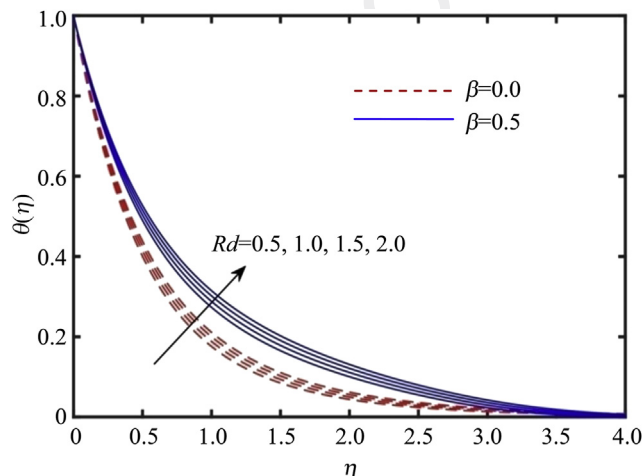


Figure 9 $\theta(\eta)$ against Rd .

wedge. Concentration distributions are boosted by enlarging We are observed from Figure 4(c).

3.4. The effect of wedge angle parameter β

Figure 5(a)–(c) indicates graphical variation in the velocity, temperature and concentration for the various values of the wedge angle parameter β along with distinct values of λ . It is noticed that the velocity, temperature and concentration enhances for higher values of β . From a physical perspective, the wedge angle parameter indicates the pressure gradient. Thus, positive values of wedge angle parameter correspond a favorable pressure gradient which enhances the flow.

3.5. Impacts of thermophoresis parameter Nt on (a) non-dimensional temperature and (b) concentration fields

The effect of thermophoresis parameter Nt on temperature and concentration are captured in Figure 6(a), (b). From the figures it is revealed that the temperature and concentration in the boundary layer has increasing behavior with an increment of Nt . From physical point of view, thermophoresis is a force in which the small particles employees physical force on other particles to move it away from hotter surface and pushed toward a colder one, and so thermal and the concentration boundary layer becomes thicker. Therefore, higher values of Nt correspond to higher thermophoretic force due to temperature gradient, which causes a rapid flow away from the wedge.

3.6. Impacts of Brownian motion parameter Nb on (a) non-dimensional temperature and (b) concentration fields

Figure 7(a), (b) divulge temperature and concentration distribution for various values of Nb . It can view from Figure 7(a) that the temperature and thermal boundary layer

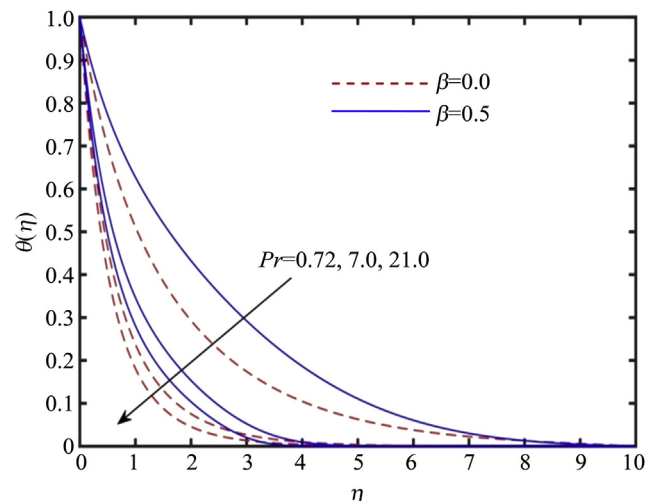


Figure 10 $\theta(\eta)$ against Pr .

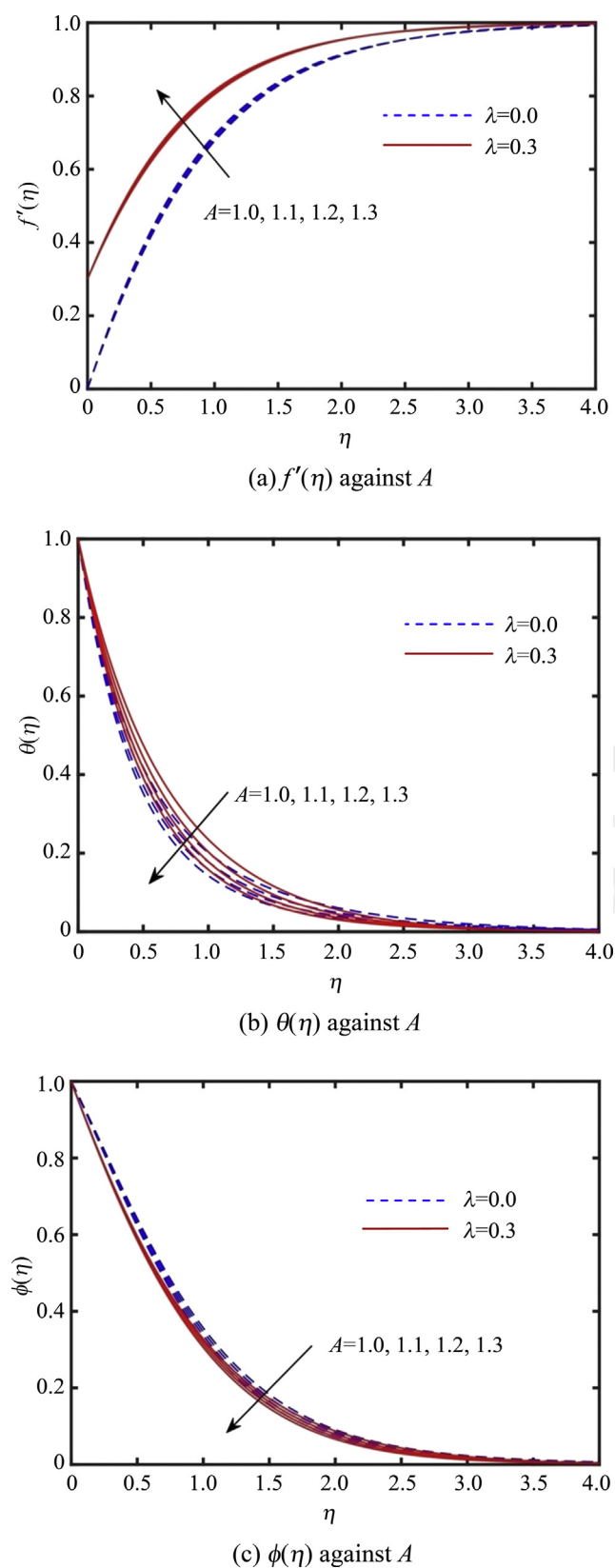


Figure 11 (a) $f'(\eta)$ against A , (b) $\theta(\eta)$ against A , and (c) $\phi(\eta)$ against A .

thickness are both escalates when Brownian motion parameter rises. The reason is that the Brownian motion exhibits heat conduction. Moreover, an enhancement in the Brownian motion boost the random motion of the particles accordingly the thermal boundary layer thickness grows. It is depicted from Figure 7(b) that a decreasing trend for growing values of Nb . As a result concentration boundary layer decreases for higher Nb .

3.7. Impacts of Le on non-dimensional concentration field

Figure 8 examines that the concentration is a decreasing function of Le . The concentration and the corresponding boundary layer thickness reduce by growing the values of Le . Since stronger Lewis number intimates a weaker Brownian diffusion coefficient which result relatively small penetration depth for the concentration boundary layer.

3.8. Impacts of radiation parameter Rd on non-dimensional temperature

The sketch between thermal fields versus horizontal axis η for varied values of the Radiation parameter Rd is shown in Figure 9. It is evident from this sketch that the temperature rises with an increase in thermal radiation parameter. This is in agreement with the physical fact that the thermal boundary layer thickness decreases with increasing Rd .

3.9. Impacts of Pr on non-dimensional temperature

Figure 10 displays the effect of Pr on dimensionless temperature profile for wedge. Fluid temperature merely reduces for increasing values of Pr . As expected, rate of thermal diffusion is lowered as Pr increases. That is, higher values of Pr lead to decrease in thermal boundary layer thickness. Consequently falls. It is also noted that the temperature is high for $\beta=0.5$ case compared with the other case.

3.10. The effect of unsteadiness parameter A

The variations of non-dimensional velocity, temperature and concentration profiles for various values of the unsteadiness parameter A are plotted in Figure 11(a)–(c). With higher unsteadiness parameter, the fluid velocity show an accelerating behavior near the solid boundary while a reverse trend is noticed when we move along η within the boundary layer regime for both the cases $\lambda=0$ (static wedge) and $\lambda=0.3$ (moving wedge). It is also noticed that the velocity and momentum boundary layer thickness are higher for $\lambda=0.3$. We further observe that the fluid temperature has declining nature for increasing A ; also the thermal boundary layer becomes thinner as in Figure 11(b). As per physics, when unsteadiness parameter rises then the wedge loses its heat and the fluid temperature decreases.

The concentration profiles are shown in Figure 11(c). From this figure, the concentration boundary layer thickness reduces with increment of A .

4. Conclusions

In the present work, the numerical solutions have been computed for the unsteady flow of Williamson fluid over a wedge with MHD and radiation. Also Blood is considered as Williamson fluid. Two fundamental cases for flow past a wedge i.e., flow over a flat plate ($\beta = 0.0$) and flow near a stagnation point ($\beta = 0.5$) have been numerically investigated in this study. The important findings of this study are as follows:

1. The thickness of the momentum boundary layer was reduced by increasing the unsteadiness parameter.
2. It is noticed that with increasing values of Hartmann number, velocity and temperature increases.
3. The effect of Brownian motion on the temperature and concentration profiles was opposite to each other.
4. An increase in thermophoresis enhance both the thermal boundary layer and concentration.
5. The velocity and temperature deprive for larger We and an opposite trend is observed for concentration.
6. The influence of radiation increases the temperature while the Pr on temperature is observed opposite.

Q4 7. An increase in Le decreases concentration.

Q5 References

- [1] R.V. Williamson, The flow of pseudoplastic materials, *Ind. Eng. Chem.* 21 (11) (1929) 1108–1111, <https://doi.org/10.1021/ie50239a035>.
- [2] S. Nadeem, S.T. Hussain, Heat transfer analysis of williamson fluid over exponentially stretching surface, *Appl. Math. Mech. Engl. Ed.* 35 (4) (2014) 489–502.
- [3] M. Khan, M.Y. Malik, T. Salahuddin, A. Hussain, Heat and mass transfer of Williamson nanofluid flow yield by an inclined Lorentz force over a nonlinear stretching sheet, *Results in Phys.* 8 (2018) 862–868, <https://doi.org/10.1016/j.rinp.2018.01.005>.
- [4] M. Khan, T. Salahuddin, M.Y. Malik, F.O. Mallawi, Change in viscosity of Williamson nanofluid flow due to thermal and solutal stratification, *Int. J. Heat Mass Transf.* 126 (2018) 941–948, <https://doi.org/10.1016/j.ijheatmasstransfer.2018.05.074>.
- [5] N.A. Khan, S. Khan, F. Riaz, Boundary layer flow of Williamson fluid with chemically reactive species using scaling transformation and homotopy analysis method, *Math. Sci. Lett.* 3 (3) (2014) 199–205.
- [6] A. Hamid, Hashim, M. Khan, Numerical investigation on heat transfer performance in time dependent flow of Williamson fluid past a wedge-shaped geometry, *Results in Phys.* 9 (2018) 479–485, <https://doi.org/10.1016/j.rinp.2018.01.025>.
- [7] Hashim, M. Khan, A. Hamid, Numerical investigation on time-dependent flow of Williamson nanofluid along with heat and mass transfer characteristics past a wedge geometry, *Int. J. Heat Mass Transf.* 118 (2018) 480–491, <https://doi.org/10.1016/j.ijheatmasstransfer.2017.10.126>.
- [8] A. Tanveer, T. Salahuddin, M. Khan, A.S. Alshomrani, M.Y. Malik, The assessment of nanofluid in a Von Karman flow with temperature relied viscosity, *Results in Phys.* 9 (2018) 916–922, <https://doi.org/10.1016/j.rinp.2018.03.051>.
- [9] P.B.A. Reddy, S. Suneetha, N.B. Reddy, Numerical study of magnetohydrodynamics (MHD) boundary layer slip flow of a Maxwell nanofluid over an exponentially stretching surface with convective boundary condition, *Propuls. Power Res.* 6 (4) (2017) 259–268, <https://doi.org/10.1016/j.jprr.2017.11.002>.
- [10] M. Khan, Hashim, Effects of multiple slip on flow of magneto-Carreau fluid along wedge with chemically reactive species, *Neural Comput. Appl.* (2016) 1–13, <https://doi.org/10.1007/s00521-016-2825-3>.
- [11] I. Khan, M.Y. Malik, A. Hussain, T. Salahuddin, Effect of homogenous-heterogeneous reactions on MHD Prandtl fluid flow over a stretching sheet, *Results in Phys.* 7 (2017) 4226–4231, <https://doi.org/10.1016/j.rinp.2017.10.052>.
- [12] A. Hussain, M.Y. Malik, M. Awais, T. Salahuddin, S. Bilal, Computational and physical aspects of MHD Prandtl-Eyring fluid flow analysis over a stretching sheet, *Neural Computing and Applications* (2017) 1–9, <https://doi.org/10.1007/s00521-017-3017-5>.
- [13] A. Hussain, M.Y. Malik, T. Salahuddin, A. Rubab, Effects of viscous dissipation on MHD tangent hyperbolic fluid over a nonlinear stretching sheet with convective boundary conditions, *Results in Phys.* 7 (2017) 3502–3509, <https://doi.org/10.1016/j.rinp.2017.08.026>.
- [14] M. Bibi, Khalil-Ur Rehman, M.Y. Malik, M. Tahir, Numerical study of unsteady Williamson fluid flow and heat transfer in the presence of MHD through a permeable stretching surface, *Eur. Phys. J. Plus.* 133 (4) (2018) 1–15, <https://doi.org/10.1140/epjp/i2018-11991-2>.
- [15] I. Ullah, I. Khan, S. Shafie, Heat and mass transfer in unsteady MHD slip flow of Casson fluid over a moving wedge embedded in a porous medium in the presence of chemical reaction: numerical solutions using Keller-Box method, *Numer. Methods Partial. Differ. Equ.* (2017) 1–25, <https://doi.org/10.1002/num.22221>.
- [16] Hashim, A. Hamid, M. Khan, U. Khan, Thermal radiation effects on Williamson fluid flow due to an expanding/contracting cylinder with nanomaterials: dual solutions, *Phys. Lett. A* 382 (30) (2018) 1982–1991, <https://doi.org/10.1016/j.physleta.2018.04.057>.
- [17] M. Khan, A. Hamid, Influence of non-linear thermal radiation on 2D unsteady flow of a Williamson fluid with heat source/sink, *Results Phys.* 7 (2017) 3968–3975, <https://doi.org/10.1016/j.rinp.2017.10.014>.
- [18] MdS. Khan, I. Karim, MdS. Islam, O. Wahiduzzaman, MHD boundary layer radiative, heat generating and chemical reacting flow past a wedge moving in a nanofluid, *Nano Converg.* (2014) 1–20, <https://doi.org/10.1186/s40580-014-0020-8>.
- [19] T. Hayat, A. Shafiq, A. Alsaedi, Hydromagnetic boundary layer flow of Williamson fluid in the presence of thermal radiation and Ohmic dissipation, *Alexandria Eng. J.* 55 (3) (2016) 2229–2240.
- [20] S. Srinivas, P.B.A. Reddy, B.S.R.V. Prasad, Effects of chemical reaction and thermal radiation on MHD flow over an inclined permeable stretching surface with non-uniform heat source/sink: an application to the dynamics of blood flow, *J. Mech. Med. Biol.* 14 (5) (2014) 1450067, <https://doi.org/10.1142/S0219519414500675>.
- [21] S.R.R. Reddy, P.B.A. Reddy, S. Suneetha, Magnetohydro dynamic flow of blood in a permeable inclined stretching viscous dissipation, non-uniform heat source/sink and chemical reaction, *Front. Heat Mass Transf.* 10 (22) (2018), <https://doi.org/10.5098/hmt.10.22>.
- [22] N.S. Akbar, S. Nadeem, C. Lee, Influence of heat transfer and chemical reactions on Williamson fluid model for blood flow through a tapered artery with a stenosis, *Asian J. Chem.* 24 (6) (2012) 2433–2441.

- 1
2
3
4
5
6
7
8
9
10
11
12
13
14
- [23] W.A. Khan, R.S.R. Gorla, Heat and mass transfer in non-Newtonian nanofluids over a non-isothermal stretching wall, *J. Nanoeng. Nanosyst.* 225 (4) (2012) 155–163.
- [24] M.S. Alam, T. Islam, M.M. Rahman, Unsteady hydromagnetic forced convective heat transfer flow of a micropolar fluid along a porous wedge with convective surface boundary condition, *Int. J. Heat Tech.* 33 (2015), <https://doi.org/10.18280/ijht.330219>.
- [25] A. Ishaq, R. Nazar, I. Pop, Moving wedge and flat plate in a micropolar fluid, *Intermt. J. Sci.* 44 (2006) 1225–1236.
- [26] R. Rajagopal, A.S. Gupta, T.Y. Na, A note on the Falkner-Skan flows of a non-Newtonian fluid, *Int. J. Non-Linear Mech.* 18 (1983) 313–320.
- [27] B.L. Kuo, Application of the differential transformation method to the solutions of Falkner-Skan wedge flow, *Acta Mech.* 164 (2003) 161–174.
- [28] M. Turkyilmazoglu, Determination of the correct range of physical parameters in the approximate analytical solutions of nonlinear equations using the adomian decomposition method, *Mediterr. J. Math.* 13 (2016) 4019–4037.
- [29] J.C. Misra, A. Sinha, Effect of thermal radiation on MHD flow of blood and heat transfer in a permeable capillary in stretching motion, *Heat Mass Transf.* 49 (2013) 617–628.
- [30] J.W. Valvano, S. Nho, G.T. Anderson, Analysis of the Weinbaum-Jiji model of blood flow in the canine kidney cortex for self-heated thermistors, *J. Biomech. Eng.* 116 (1999) 201–207.
- [31] J.C. Chato, Heat transfer to blood vessels, *J. Biomech. Eng.* 102 (1980) 110–118.
- 15
16
17
18
19
20
21
22
23
24
25
26
27
28

UNCORRECTED PROOF